



ARTICLE

Facile Preparation of Fe–N–C Oxygen Reduction Electrocatalysts from Metal Organic Frameworks for Zn–Air Battery

Chengcheng Wang^{1,2,*}, Dawei Luo¹, Bingxue Hou³, Mortaza Gholizadeh⁴, Zanxiong Tan¹ and Xiaojie Han¹

¹Shenzhen Polytechnic, Shenzhen, China

²Key Laboratory of Energy Conversion and Storage Technologies (Southern University of Science and Technology), Ministry of Education Shenzhen, Shenzhen, China

³Aviation Engineering Institute, Civil Aviation Flight University of China, Guanghan, China

⁴Faculty of Chemical and Petroleum Engineering, University of Tabriz, Tabriz, Iran

*Corresponding Author: Chengcheng Wang. Email: sabrinachch_123@hotmail.com

Received: 16 August 2021 Accepted: 18 September 2021

ABSTRACT

It is critical to study efficient, stable oxygen reduction reaction (ORR) electrocatalysts due to insufficient stability and expensive price of Pt/C catalysts for Zn-air batteries. Fe–N–C electrocatalysts was synthesized by a facile solvent-green method and the efficiency of Fe–N–C optimized was studied as potential ORR electrocatalysts under alkaline condition. Results indicated that it had excellent ORR activity with $E_{1/2}$ of 0.93 V, which was competitive to that of Pt/C-JM under the same conditions. Moreover, the assembled Zn-air battery exhibited discharge potential and charge potential of 1.2 V, 2.32 V at 5 mA cm^{-2} with high stability, respectively. Overall, all results illustrated that Fe–N–C is an excellent ORR electrocatalyst in the field of metal air battery. Additionally, this work opens a good way to synthesize highly efficient electrocatalysts from metal organic framework and to investigate ORR mechanism of efficient chemical energy to electricity conversion.

KEYWORDS

Manuscript; Fe–N–C electrocatalyst; oxygen reduction reaction; Zn-air battery

1 Introduction

Zinc-air battery has been paid much attention as an energy storage device due to its high energy density, safety, environmental protection as well as economic costs [1–4]. Oxygen reduction reaction (ORR) is largely hampered because of the slow kinetics as well as high overpotential [5]. Until now, Pt has been recognized as the most efficient ORR electrocatalyst. However, its high cost and scarcity greatly restricted the wide commercialization for Zinc-air battery [6]. Hence, it is urgent to develop non-platinum substances to replace Pt electrocatalysts such as nitrogen coordinated metals into carbon nanomaterials. Among what has been mentioned above, Fe–N–C electrocatalysts are reckoned as one of the most practicable electrocatalysts because of their low cost, high electronic conductivity as well as high electrocatalytic activity [7–12].



Metal–organic frameworks (MOFs) are widely adopted as precursors for Fe–N–C electrocatalysts due to their strong interactions between Fe and N atoms. Zeolitic imidazolate frameworks (ZIFs) have been extensively studied because of high content of N/C, high surface area and highly dispersed metal active sites [13–27]. Wang et al. [28] studied the Fe–N–C electrocatalyst prepared by pyrolysis of solid DCDA and ammonium ferric citrate precursor. Results showed that it exhibited good bifunctional ORR and OER activities under alkaline condition compared to commercial Pt/C and IrO₂, in which exhibited maximum power density of 220 mW/cm² at 0.72 V and good cycle durability in Zinc-air battery. Recently, Chen et al. [29] studied the Fe–N–C electrocatalyst prepared by converting modified Fe-phenanthroline into Fe-NCDNA using methanol as solution. They concluded that Zn-air battery delivered maximum power density of 184 mW/cm². There are still some controversial issues regarding to ORR mechanism of Fe–N–C electrocatalysts such as Fe–N_x active sites, Fe₃O₄, different kinds of N site and so on. Li et al. [30] studied Fe–N–C by iron porphyrins precursor and found that porphyrin could adjust iron chemical states into Fe or Fe₂O₃. However, Xu et al. [31] recently reported that Fe–N–C electrocatalyst synthesized by ZIF-8 exhibited excellent ORR activity under alkaline condition, and demonstrated relatively good peak power density of 118.05 mW/cm² in Zinc-air battery. They pointed out that Fe₃O₄ could enhance the wettability of composite, in which could improve O₂ adsorption and the triple-phase boundary.

It is worth mentioning that the preparation of MOF precursors is usually done in organic solution such as methanol, N,N-Dimethyl formamide, etc. in which can result in the pollution of environment and lead to high cost. Moreover, the addition of chemicals like reducing agent can make preparation process more complicated although it can enhance electrocatalytic performance of materials. There were extensive methods regarding to the synthetic ways, it is still necessary to replace the use of organic solvents and surfactants during the preparation, which is mainly due to the numerous waste and environmental pollution. Moreover, there are still a lot to be done to understand ORR mechanism of Fe–N–C based electrocatalysts. Hence, it is vital to develop facile green method to prepare Fe–N–C electrocatalyst by using water to simplify the preparation procedure.

In this work, ZIFs were of particularly used due to their high nitrogen/carbon contents, high microporous surface area, tunable pore texture, as well as the highly dispersed metal sites even after thermal decomposition. Moreover, in order to make preparation procedure more sustainable, water was innovatively used as aqueous solution in the facile and one-pot preparation of Fe–N–C electrocatalysts. The effect of Zn:Fe mole ratio and the temperature were systematically studied to identify the electrocatalytic performance of Fe–N–C. Results showed that Fe–N–C catalyst fired at 800°C in N₂ atmosphere had high ORR activity with E_{1/2} of 0.93 V under O₂-saturated 0.1 M KOH, which was comparable with commercial Pt/C from JM (Johnson Matthey) under the same testing condition. Assembled initial Zn-air battery by Fe–N–C exhibited relatively high specific capacity and power density. This work opens light on a facile method to prepare Fe–N–C electrocatalyst and enhance its application of Zinc-air battery.

2 Experimental

2.1 Synthesis

In the first stage, a certain mole ratio of ZnNO₃ and FeNO₃ was mixed with 30 mL distilled water, and then 2-methylimidazole (2-mim) was added into the solution equipped with stirring. The mixing was continued for 24 h at room temperature. All chemicals were ordered from Sigma. Then, the solution was centrifuged with distilled water for three times at a speed of 6000 rpm and dried at 60°C in oven. Then, the precursor was sintered at 800°C for 3 h in the presence of N₂ atmosphere. The mole ratio of Fe to Zn was set at 1:2, 1:1 and 2:1 to investigate the Fe mole ratio on electrocatalytic performance of catalysts. Samples obtained were named as Fe–N–C-1# (n_(Fe) to n_(Zn)=1:2), Fe–N–C-2# (n_(Fe) to n_(Zn)=1:1), Fe–N–C-3#(n_(Fe) to n_(Zn)=2:1), respectively. For comparison, the precursor was also sintered at 1000°C to study

temperature effect on the electrocatalytic performance of catalysts, which was marked as Fe–N–C-4#, and the mole ratio of Fe to Zn was set at 1:1 (n_{Fe} to $n_{\text{Zn}} = 1:2$) as well.

2.2 Catalyst Characterization

XRD (Bruker, D8 Advances) was used to test the phase of prepared samples by $5\text{--}80^\circ$ (2θ). The samples were analyzed by XPS (Thermo Fisher company, ESCALAB 250Xi instrument). SEM from ZEISS was used to characterize prepared powders morphology. TEM and EDS were conducted by Titan G2 60–300 microscope.

2.3 Electrochemical Test

ORR activity was tested by Princeton electrochemical workstation with RDE system. Cell was made by Pt wire, saturated calomel electrodes (SCE), and catalyst was dipped into glassy carbon (working electrode). Analytical grade KOH was used as the electrolyte solution. Catalyst inks (10 mg/ml) were prepared by mixing catalyst powder (10.0 mg) including 0.1 mL Nafion solution (5 wt%), 0.9 mL ethanol to obtain homogeneous inks. In the next step, the solution was dried for 5 min. Ink (5 μL) was dipped into glassy carbon disk electrode to form uniform thin film on the working electrode. Linear scan voltammetry (LSV) was used in O_2 -saturated 0.1 M KOH from 400 to 2500 rpm at 10 mV/s from -1 to 0 V (vs. RHE). Tafel curve was also obtained under the same condition. Chronopotentiometry data was conducted at 0.75 V. IR correction was performed. The results were shown is somewhere else [32]. Pt/C-JM was tested under the same condition. The detailed information can be found in our previous published paper [33].

2.4 Battery Assembly and Test

Catalyst inks were prepared as mentioned above and then it was distributed uniformly on carbon cloth with Ni-foam (current collector). Then, carbon cloth (cathode) and polished zinc plate (anode) were assembled in Zn air battery by 6 M KOH including 0.2 M ZnCl_2 . The detailed schematic diagram is shown in Fig. 1.

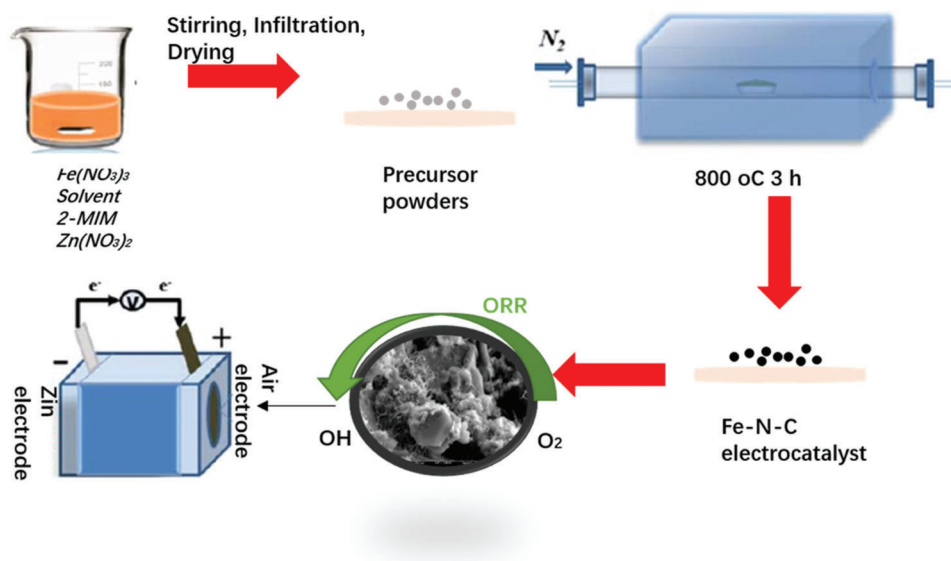


Figure 1: Schematic diagram of ORR diagram for Fe–N–C-based electrocatalysts and the assembling of Zn-air battery

Aqueous Zn air battery tests were carried out by LAND CT2001A testing device. Charge and discharge data were obtained at 5 mA cm^{-2} . Polarization curves for discharge process were collected by CHI6000A at 0.5 mA/s .

3 Results and Discussion

3.1 Phase and Microstructure Characterization

XRD patterns for Fe–N–C-1# to Fe–N–C-4# electrocatalysts after firing were shown in Fig. 2. All four samples included two broad peaks at 25° and 43° , which were responded to graphitized and amorphous carbon, respectively. Peaks did not change with preparation temperature, which increased to 1000°C . Results indicated that the temperature had little effect on graphitized carbon formation. For Fe–N–C-3# (Fig. 2c), graphitized carbon was detected, moreover, two peaks (PDF card: #06-0627) were located at 40° and 48° , and its space group was Pm-3m (221) with $a = b = c = 3.795 \text{ nm}$. These two peaks were correlated to Fe_4N phase.

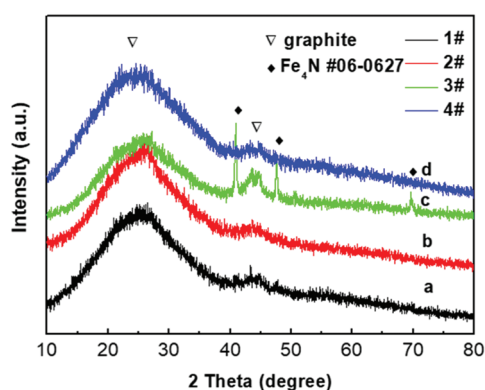


Figure 2: XRD of Fe–N–C-1# to Fe–N–C-4# catalysts (a–d)

Fig. 3 exhibits SEM images of the catalysts for Fe–N–C-1# to Fe–N–C-4# electrocatalysts. There was an obvious morphology difference for four samples. More obvious carbon nanotube structures can be observed for samples Fe–N–C-2#. Fe–N–C electrocatalysts were also prepared by solid-phase preparation in our previous reported paper [33], in which reported that obvious carbon nanotube structures could be found and the formation of carbon nanotube structures can greatly benefit active site and enhance ORR activity and stability. It is also obvious that when the temperature increased to 1000°C , nanoparticles became bigger and the structure was much denser than other three samples (Figs. 3a and 3h). It can also be observed that fewer carbon nanotube structures were detected in Figs. 3a and 3h. Compared to Fe–N–C-2# that was prepared at lower temperature (800°C), the Fe–N–C-4# sample was probably showing relatively lower electrochemical performance. So it is essential to adjust catalyst morphology and the synthesis temperature to improve catalytic performance. Fig. 4 shows typical TEM images for Fe–N–C-2# catalysts. Porous carbon structure can be observed in high magnified images (Fig. 4a). Moreover, carbon nanotube shape can also be observed. Elemental mapping by TEM identifies that C, N and Fe elements were distributed homogeneously within the structure. Results could indicate that Fe existed in Fe–N–C-2# catalysts in a highly dispersed state.

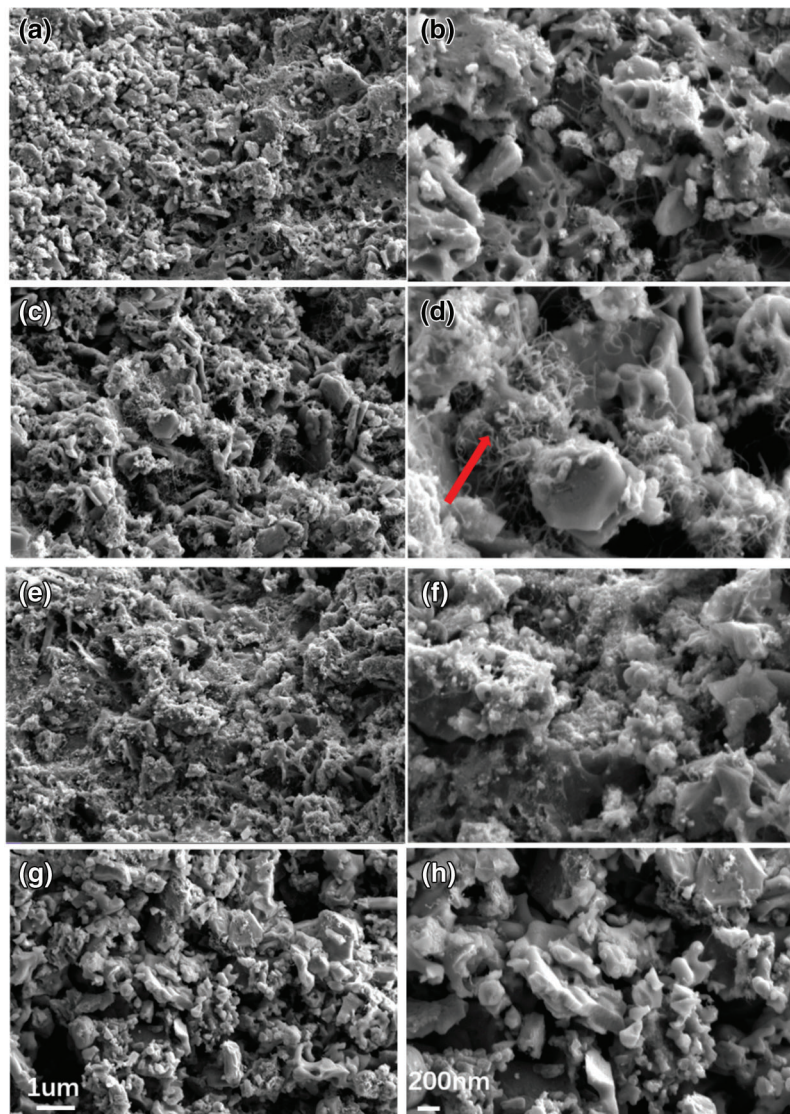


Figure 3: SEM images of Fe-N-C-1# (a, b), Fe-N-C-2# (c, d), Fe-N-C-3# (e, f) and Fe-N-C-4# catalysts (g, h)

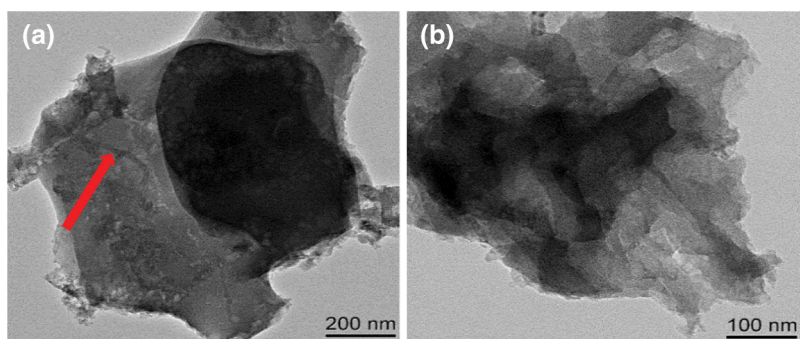


Figure 4: Continued

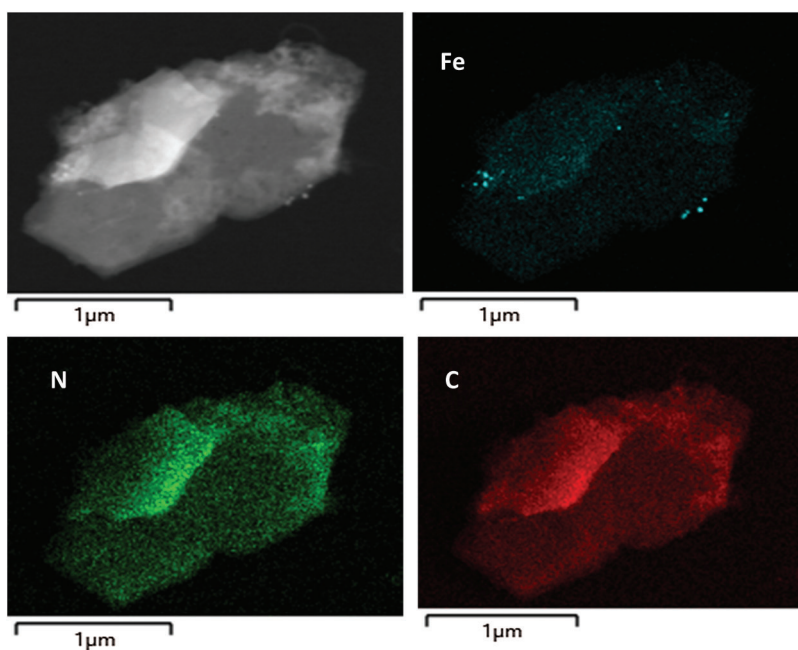


Figure 4: TEM images of Fe–N–C-2# catalysts (a–b) and elemental mapping of Fe–N–C-2# catalysts in the corresponding region

Survey scan of the catalysts for the four Fe–N–C electrocatalysts shown in Fig. 5, which can indicate the presence of N, C, Fe elements. XPS results indicated that Fe was found in Fe–N–C-2# with peak at 710 eV. It shows strong reaction between Fe and N, C. This result was similar with carbon morphology in TEM. Fe was coordinated by four N atoms from 2-mim, which was beneficial for forming FeN_x sites into porous carbon substrate by thermal conversion.

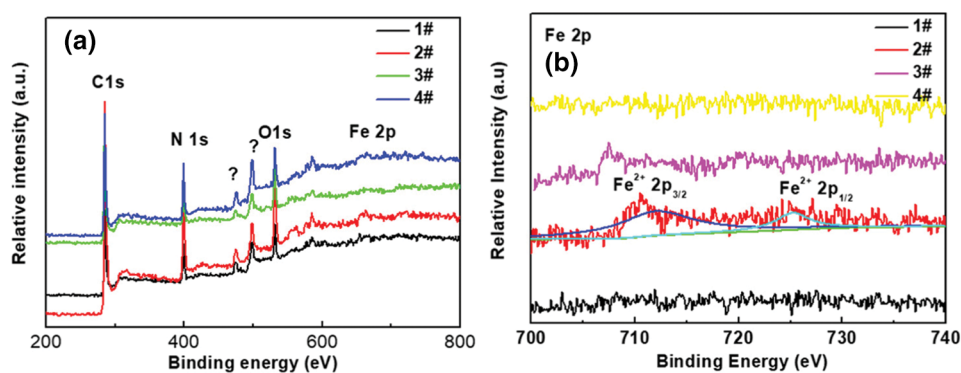


Figure 5: Continued

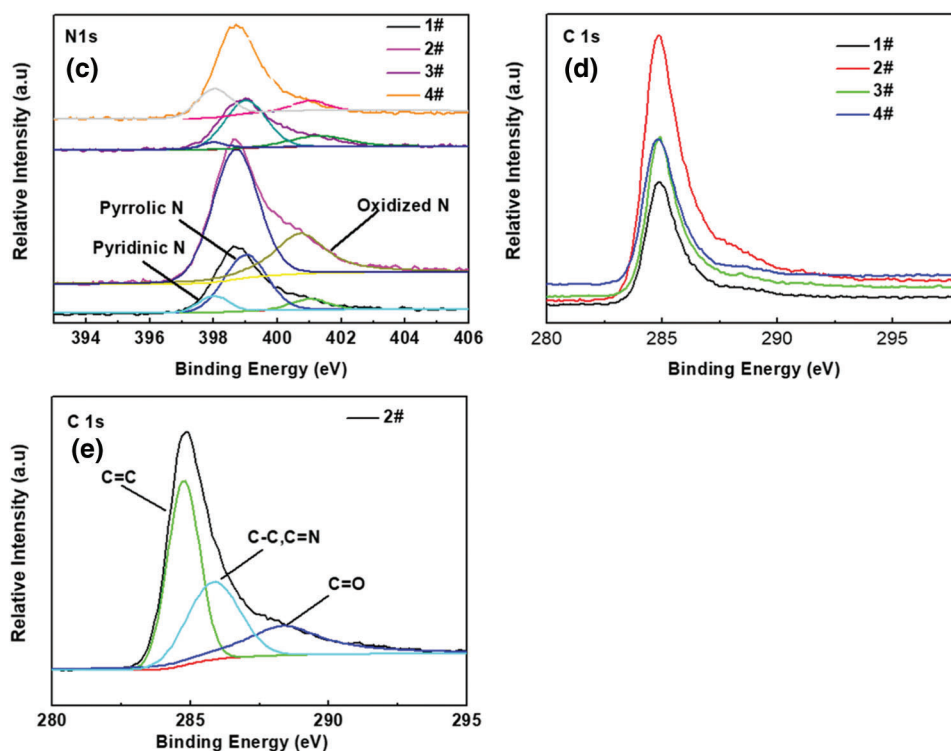


Figure 5: Selected XPS survey (a) of Fe–N–C-1#, Fe–N–C-2#, Fe–N–C-3# and Fe–N–C-4# catalysts. High resolution Fe 2p (b), N 1s (c), C 1s (d) of XPS spectra, deconvoluted C 1s (e) of Fe–N–C-2# XPS spectra

Deconvolution of Fe 2p in Fe–N–C-2# could indicate that Fe 2p_{3/2} and Fe 2p_{1/2} peaks appeared at 780 and 796 eV were related to Fe²⁺ oxidation state. Deconvolution of C 1s in Fe–N–C-2# was composed of C=C, C–C, C=N, and C=O [34]. Table 1 lists comparison of total C content for Fe–N–C-2# catalysts after deconvolution. C=C, C–C provided sufficient substrate for electronic conduction, and C=O stemmed from C–O–Fe. Possibly, C=N served as active sites of ORR. All four samples contained nitrogen. Deconvolution of N 1s XPS spectra was assigned to two compositions regarding to pyridinic nitrogen of 398 eV, pyrrolic nitrogen of 399 eV and oxidized nitrogen of 401 eV [34]. Very recently, pyridinic N could improve electronic structure of carbon atom around, which could be related to the active sites leading to the enhanced ORR performance. The active group could take up more than 80% of total N atoms in Fe–N–C-2# as shown in Table 2. Higher content of pyridinic N and pyrrolic N was promising due to higher positive charge density and enhancing current density by promoting oxygen adsorption and weakening O–O bonds. Pyridinic nitrogen could react with Fe to form Fe–N_x, which was more active in ORR.

Table 1: Comparison of total C content for Fe–N–C-2# catalysts after deconvolution

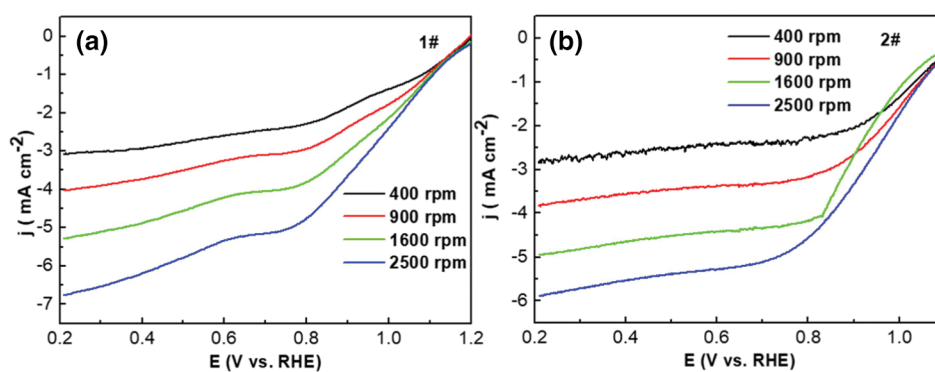
C 1s	C=C	C=O	C–C, C=N
Fe–N–C-2#	284.7 eV	288.34 eV	285.82 eV
percentage	44.29%	25.38%	30.33%

Table 2: Comparison of total N content and pyridinic N, oxidized N, graphitic N for Fe–N–C-1# to Fe–N–C-4# catalysts after deconvolution

N 1s	Pyrolic N	Oxidized N	Pyridinic N
Fe–N–C-1#	399 eV	401 eV	398 eV
percentage	72.48%	12.36%	15.16%
Fe–N–C-2#	398.7 eV	400.7 eV	/
percentage	80.66%	19.34%	/
Fe–N–C-3#	398.9 eV	401.3 eV	397.99 eV
percentage	68.29%	23.19%	8.52%
Fe–N–C-4#	399 eV	401 eV	398 eV
percentage	70.05%	17.89%	12.06%

3.2 Electrocatalytic Performance

Fig. 6 illustrates ORR activity of Fe–N–C-1# to Fe–N–C-4# electrodes under O₂–0.1 M KOH at 10 mV/s by different rotating speeds. E_{onset} of Fe–N–C-2# was 0.97 V, while E_{1/2} was 0.93 V. As Fe:Zn mole ratio decreased to 1:2, E_{onset} and E_{1/2} of Fe–N–C-1# were 0.98 and 0.919 V, respectively. However, when Fe:Zn mole ratio increased to 2:1, E_{onset} and E_{1/2} of Fe–N–C-3# decreased to 0.95 and 0.75 V, respectively. When the temperature increased to 1000°C, E_{onset} and E_{1/2} of Fe–N–C-4# reached to 0.92 and 0.74 V. For commercial Pt/C, E_{onset} and E_{1/2} were 0.98, 0.93 V, respectively. One of the main reasons that Fe–N–C-2# could exhibit excellent electrocatalytic activities was due to more obvious carbon nanotube structures can be observed, in which can greatly benefit active site and enhance ORR activity and stability. Another reason might be due to XPS results of N peak, and it might be concluded that the relatively large amount of pyridinic nitrogen and pyrrolic N were closely correlated by enhancing current density and oxygen adsorption and weakening of O–O bonds. Therefore, it could lead to the superior ORR activities. The linearity of K-L curves was calculated in our previous published paper [33], which could identify real direct 4-electron reduction. Chronopotentiometry ORR stability for Fe–N–C-2# was studied at 0.75 V (Fig. 6f) with same loading condition. Fe–N–C-2# showed superior ORR stability. It initially reached at 4.81 mA/cm² and then became 4.89 mA/cm² after 10000 s. These results showed the remarkable performance of Fe–N–C-2# as nonprecious metal catalysts with remarkable ORR activity and stability.

**Figure 6:** Continued

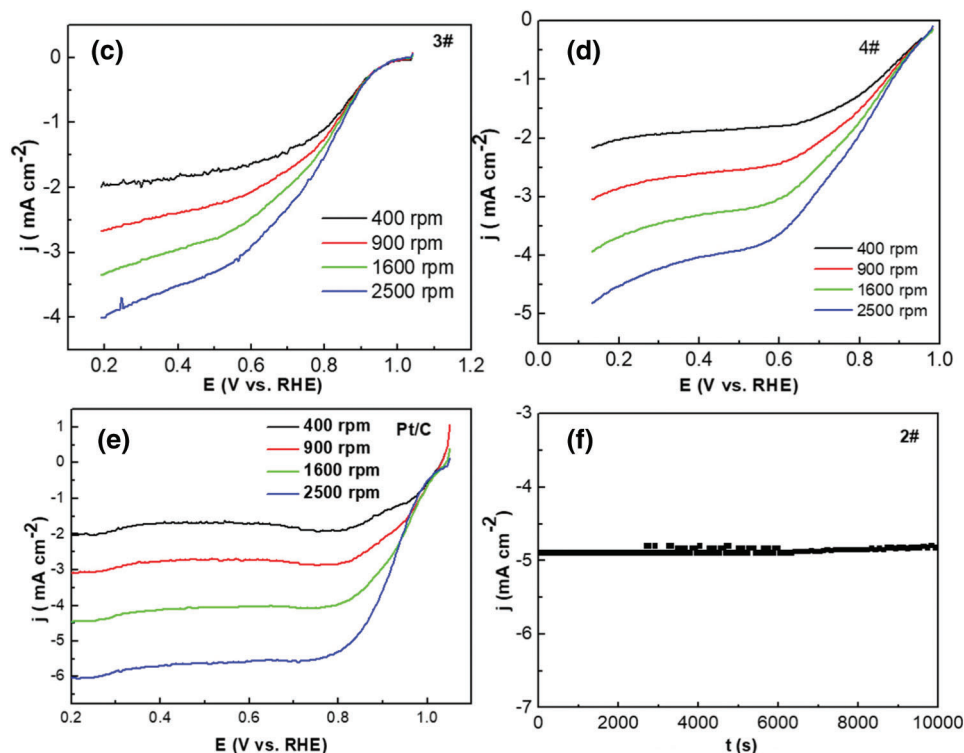


Figure 6: Linear sweep voltammetry (LSV) for oxygen reduction of Fe–N–C-1# (a), Fe–N–C-2# (b), Fe–N–C-3# (c) and Fe–N–C-4# catalysts (d), Pt/C-JM (e) in O₂ saturated 0.1 M KOH at different rotation speeds and scan rate of 5 mV/s. Current-time chronoamperometric response of for Fe–N–C-2# catalysts under 1600 rpm in O₂ saturated 0.1 M KOH at 0.75 V (f)

3.3 Cell Performance

Practical applicability of Fe–N–C-2# electrocatalyst was tested in aqueous Zn air battery. Three Zn air batteries were assembled together to obtain open circuit voltage (OCV) at 3.62 V (Fig. 7a). The average OCVs of Fe–N–C-2#-based Zn air battery was around 1.21 V from polarization profiles (Fig. 7c). Zn air battery exhibited peak power density of 80 mW/cm² at 150 mA cm⁻², which was 19.2 mW/cm² lower than that of reported paper [31], and the performance of the cell was still needed to be optimized. Fig. 7b shows the stability of Zn air battery, which was evaluated by charging for 10 mins and discharging for 10 mins over repeated cycles at 5 mA cm⁻². Initially, it showed discharge potential and charge potential of 1.20 and 2.32 V. Therefore, it could be calculated that the voltage gap ($\Delta\eta$) was 1.12 V. After 48 h, voltage gap increased to 1.4 V, respectively. Such phenomenon was probably due to the irreversible Zn plating–stripping process. It is obvious that Fe–N–C-2#-Zn-air battery has promising recharge ability, and its performance is comparable to the results reported in the paper [34]. Fe–N–C-2# is cheaper than 20 wt %-Pt/C, in which shows its high economic potential. Fig. 8 shows SEM image of the Fe–N–C-2# Zn-air battery after long term test. There was obvious microstructure change after the test and some residual of Zn, S, Na, K, F element could also be observed after cycling.

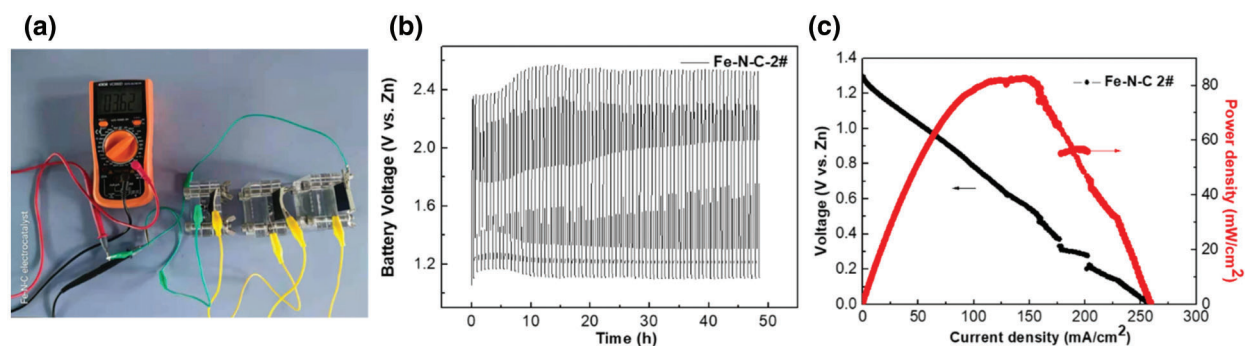


Figure 7: a) OCV for Fe–N–C-2# assembled-Zn air batteries. b) Galvanostatic charge–discharge profiles of Zn air batteries at 5 mA cm^{-2} . c) I–V and P–V curves for assembled-Zn air batteries

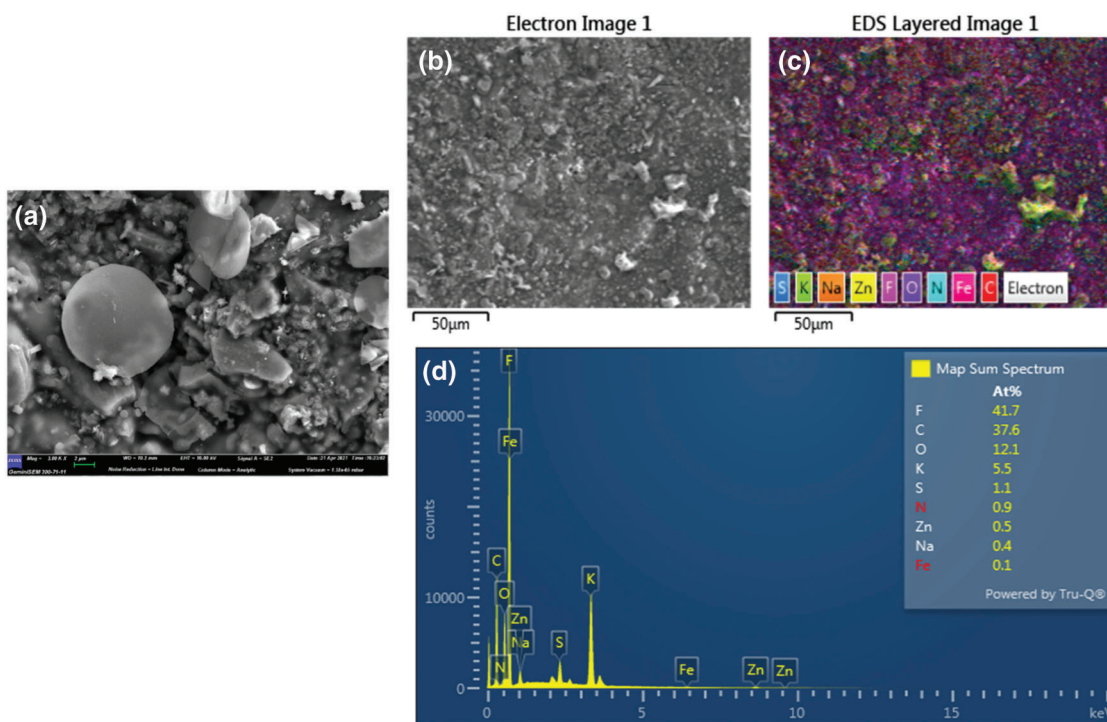


Figure 8: Surface SEM image (a, b) and mapping (c), EDX (d) of the Fe–N–C-2#-Zn-air battery after long term test

4 Conclusions

In conclusion, highly efficient Fe–N–C electrocatalysts with active Fe–N₄ sites were successfully prepared by a facile green solvent approach and adopted as a potential ORR electrode in Zn-air battery. Optimized Fe–N–C electrocatalysts exhibited excellent ORR activity with $E_{1/2}$ of 0.93 V. Moreover, it had high durability, better Zn-air battery discharge performance and high cycle stability. Excellent performance could be due to the efficient mass transferring, high Fe–N₄ active sites, carbon nanotube structure and high electronic conductivity. The results clarified a facile green solution processing way to prepare non-platinum electrocatalysts of energy storage devices.

Acknowledgement: The authors acknowledge the facilities, the scientific and technical assistance from Hoffman Research Institute in Shenzhen Polytechnic.

Funding Statement: Authors received the funding from 2021 Special Innovative Talents Project by Education Department of Guangdong Province.

Conflicts of Interest: The authors declare that they have no conflicts of interest to report regarding the present study.

References

1. Cao, R., Lee, J. S., Liu, M. L., Cho, J. (2012). Recent progress in non-precious catalysts for metal–air batteries. *Advanced Energy Materials*, 2(7), 816–829. DOI 10.1002/aenm.201200013.
2. Li, H. F., Ma, L. T., Han, C. P., Wang, Z. F., Liu, Z. X. et al. (2019). Advanced rechargeable zinc-based batteries: Recent progress and future perspectives. *Nano Energy*, 62, 550–587. DOI 10.1016/j.nanoen.2019.05.059.
3. Pan, J., Xu, Y. Y., Yang, H., Dong, Z. H., Liu, H. F. et al. (2018). Advanced architectures and relatives of air electrodes in Zn-air batteries. *Advanced Science*, 5, 4. DOI 10.1002/advs.201700691.
4. Park, J., Park, M., Nam, G., Lee, J. S., Cho, J. (2015). All-solid-state cable-type flexible Zinc–air battery. *Advanced Materials*, 27, 1396. DOI 10.1002/adma.201404639.
5. Shao, M., Chang, Q., Dodelet, J. P., Chenitz, R. (2016). Recent advances in electrocatalysts for oxygen reduction reaction. *Chemical Reviews*, 116, 3594–3657. DOI 10.1021/acs.chemrev.5b00462.
6. Debe, M. K. (2012). Electrocatalyst approaches and challenges for automotive fuel cells. *Nature*, 486, 43. DOI 10.1038/nature11115.
7. Lefevre, M., Proietti, E., Jaouen, F. D., Jaouen, J. P. (2009). Iron-based catalysts with improved oxygen reduction activity in polymer electrolyte fuel cells. *Science*, 324, 71–74. DOI 10.1126/science.1170051.
8. Wu, G., More, K. L., Johnston, C. M., Zelenay, P. (2011). High-performance electrocatalysts for oxygen reduction derived from polyaniline, iron, and cobalt. *Science*, 332, 443–447. DOI 10.1126/science.1200832.
9. Pan, Y., Liu, S., Sun, K., Chen, X., Wang, B. et al. (2018). A bimetallic Zn/Fe polyphthalocyanine-derived single-atom FeN₄ catalytic site: A superior trifunctional catalyst for overall water splitting and Zn-air batteries. *Angewandte Chemie International Edition*, 130, 8750–8754. DOI 10.1002/ange.201804349.
10. Chen, Y., Li, Z., Zhu, Y., Sun, D., Liu, X. et al. (2019). Atomic Fe dispersed on N-doped carbon hollow nanospheres for high-efficiency electrocatalytic oxygen reduction. *Advanced Materials*, 31, 1806312. DOI 10.1002/adma.201806312.
11. Jasinski, R. (1964). A new fuel cell cathode catalyst. *Nature*, 201, 1212–1213. DOI 10.1038/2011212a0.
12. He, W., Wang, Y., Jiang, C., Lu, L. (2016). Structural effects of a carbon matrix in non-precious metal O₂-reduction electrocatalysts. *Chemical Society Reviews*, 45, 2396–2409. DOI 10.1039/C5CS00665A.
13. Wan, X., Wu, R., Deng, J., Nie, Y., Chen, S. et al. (2018). A metal-organic framework derived 3D hierarchical Co/N-doped carbon nanotube/nanoparticle composite as an active electrocatalyst for oxygen reduction in alkaline electrolyte. *Journal of Materials Chemistry A*, 6, 3386–3390. DOI 10.1039/C7TA10022A.
14. Li, Z., Sun, H., Wei, L., Jiang, W. J., Wu, M. et al. (2017). Lamellar metal organic framework-derived Fe–N–C non-noble electrocatalysts with bimodal porosity for efficient oxygen reduction. *ACS Applied Materials & Interfaces*, 9, 5272–5278. DOI 10.1021/acsami.6b15154.
15. Lai, Q., Zheng, L., Liang, Y., He, J., Zhao, J. et al. (2017). Meta-organic-framework-derived Fe–N/C electrocatalyst with five-coordinated Fe–N–x sites for advanced oxygen reduction in acid media. *ACS Catalysis*, 7, 1655–1663. DOI 10.1021/acscatal.6b02966.
16. Ai, K., Li, Z., Cui, X. (2017). Scalable preparation of sized-controlled Co–N–C electrocatalyst for efficient oxygen reduction reaction. *Journal of Power Sources*, 368, 46–56. DOI 10.1016/j.jpowsour.2017.09.067.
17. Wu, H. B., Lou, X. W. (2017). Metal-organic frameworks and their derived materials for electrochemical energy storage and conversion: Promises and challenges. *Science Advances*, 3, 9252. DOI 10.1126/sciadv.aap9252.

18. Li, Y., Xu, Y., Yang, W., Shen, W., Xue, H. et al. (2018). MOF-Derived metal oxide composites for advanced electrochemical energy storage. *Small*, *14*, 1704435. DOI 10.1002/sml.201704435.
19. Cao, X., Tan, C., Sindoro, M., Zhang, H. (2017). Hybrid micro-/nano-structures derived from metal-organic frameworks: Preparation and applications in energy storage and conversion. *Chemical Society Reviews*, *46*, 2660–2677. DOI 10.1039/C6CS00426A.
20. Dissegna, S., Epp, K., Heinz, W. R., Kieslich, G., Fischer, R. A. (2018). Defective metal-organic frameworks. *Advanced Materials*, *30*, 1704501. DOI 10.1002/adma.201704501.
21. Jiao, L., Wang, Y., Jiang, H. L., Xu, Q. (2018). Metal-organic frameworks as platforms for catalytic applications. *Advanced Materials*, *30*, 1703663. DOI 10.1002/adma.201703663.
22. Wang, S., McGuirk, C. M., d’Aquino, A., Mason, J. A., Mirkin, C. A. (2018). Metal-organic framework nanoparticles. *Advanced Materials*, *30*, 1800202. DOI 10.1002/adma.201800202.
23. Yuan, S., Feng, L., Wang, K., Pang, J., Bosch, M. et al. (2018). Stable metal–organic frameworks: Design, synthesis, and applications. *Advanced Materials*, *30*, 1704303. DOI 10.1002/adma.201704303.
24. Yang, L., Kong, J., Zhou, D., Ang, J. M., Phua, S. L. et al. (2014). Transition-metal-ion-mediated polymerization of dopamine: Mussel-inspired approach for the facile synthesis of robust transition-metal nanoparticle–Graphene hybrids. *Chemistry—A European Journal*, *20*, 7776–7783. DOI 10.1002/chem.201402241.
25. Tang, J., Salunkhe, R. R., Liu, J., Torad, N. L., Imura, M. et al. (2015). Thermal conversion of core-shell metal-organic frameworks: A new method for selectively functionalized nanoporous hybrid carbon. *Journal of the American Chemical Society*, *137*, 1572–1580. DOI 10.1021/ja511539a.
26. Chen, Y. Z., Wang, C., Wu, Z. Y., Xiong, Y., Xu, Q. et al. (2015). From bimetallic metal-organic framework to porous carbon: High surface area and multicomponent active dopants for excellent electrocatalysis. *Advanced Materials*, *27*, 5010–5016. DOI 10.1002/adma.201502315.
27. Niu, Q., Guo, J., Chen, B., Nie, J., Guo, X. et al. (2017). Bimetal-organic frameworks/polymer core-shell nanofibers derived heteroatom-doped carbon materials as electrocatalysts for oxygen reduction reaction. *Carbon*, *114*, 250–260. DOI 10.1016/j.carbon.2016.12.016.
28. Wang, J., Wu, H. H., Gao, D. F., Miao, S., Wang, G. X. et al. (2015). High-density iron nanoparticles encapsulated within nitrogen-doped carbon nanoshell as efficient oxygen electrocatalyst for zinc-air battery. *Nano Energy*, *13*, 387–396. DOI 10.1016/j.nanoen.2015.02.025.
29. Chen, K., Ci, S. Q., Xu, Q. H., Cai, P. W., Li, M. Z. et al. (2020). Iron-incorporated nitrogen-doped carbon materials as oxygen reduction electrocatalysts for Zinc-air batteries. *Chinese Journal of Catalysis*, *41*, 858–867. DOI 10.1016/S1872-2067(19)63507-2.
30. Li, Z., Wei, L., Jiang, W. J., Hu, Z., Luo, H. et al. (2019). Chemical state of surrounding iron species affects the activity of Fe–Nx for electrocatalytic oxygen reduction. *Applied Catalysis B*, *251*, 240–246. DOI 10.1016/j.apcatb.2019.03.046.
31. Xu, K. F., Bao, H. Y., Tang, C. Y., Maliutina, K., Li, F. J. et al. (2020). Engineering hierarchical MOFs-derived Fe–N–C nanostructure with improved oxygen reduction activity for Zinc-air battery: The role of iron oxide. *Materials Today Energy*, *18*, 100500. DOI 10.1016/j.mtener.2020.100500.
32. Wang, C. C., Hou, B. X., Wu, X. F., Fan, X., Cui, X. (2019). Efficient bimetallic zeolitic imidazolate framework derived Co–N–C oxygen reduction reaction electrocatalysts. *Materials Research Express*, *6*, 12. DOI 10.1088/2053-1591/ab573b.
33. Hou, B. X., Wang, C. C., Tang, R., Zhang, Q., Cui, X. M. (2020). High performance Fe–N–C oxygen reduction electrocatalysts by solid-phase preparation of metal-organic frameworks. *Materials Research Express*, *7*, 025506. DOI 10.1088/2053-1591/ab70e3.
34. Li, B., Sasikala, S. P., Kim, D. H., Bak, J., Kim, I. et al. (2019). Fe–N₄ complex embedded free-standing carbon fabric catalysts for higher performance ORR both in alkaline & acidic media. *Nano Energy*, *56*, 524–530. DOI 10.1016/j.nanoen.2018.11.054.